Chemical Science

ROYAL SOCIETY OF CHEMISTRY

EDGE ARTICLE

View Article Online
View Journal

Cite this: DOI: 10.1039/d6sc00337k

All publication charges for this article have been paid for by the Royal Society of Chemistry

Cooperative reactivity of halomethanes and -silanes at an A-frame complex: transannular addition *versus* bridging tetrylenes

Max Passargus,[ab] Celine Nieuwland,[c] Merle Arrowsmith,[ab] F. Matthias Bickelhaupt *[cde] and Holger Braunschweig *[ab]

With CH_2X_2 (X = Cl, Br, I) and CCl_4 the diplatinum(0) complex [(μ-dmpm)$_2$Pt$_2$(nbe)$_2$] (dmpm = bis(dimethylphosphino)methane, nbe = norbornene) undergoes facile cooperative addition of one C–X bond at each Pt centre to yield the methylene-bridged diplatinum(II) A-frame complexes [(μ-dmpm)$_2$Pt$_2$X$_2$(μ-CY$_2$)] (Y=H, Cl). In contrast, reactions with $Me_{4-n}SiX_n$ (X = Cl, n = 1–3; X = I, n = 1) lead preferentially to transannular oxidative additions of a single Si–X bond over the two metal centres, yielding the complexes [(μ-dmpm)$_2${PtX}{Pt(SiMe$_{4-n}$X$_{n-1}$)}]. In CH_2Cl_2 [(μ-dmpm)$_2${PtCl}{Pt(SiCl$_3$)}] undergoes rearrangement to the silylene-bridged [(μ-dmpm)$_2$Pt$_2$Cl$_2$(μ-SiCl$_2$)], while in CH_2Br_2 oxidation of the platinum centres to Pt(II), Cl–Br exchange, and the insertion of a CH_2Br_2-derived methylene unit into the Pt–Si bond are observed. Quantum-chemical calculations provide insights into the differences in reactivity between the halomethanes and -silanes.

Received 13th January 2026
Accepted 3rd April 2026

DOI: 10.1039/d6sc00337k

rsc.li/chemical-science

Introduction

The oxidative addition of polar carbon–halogen bonds to electron-rich metal complexes is a key step in many examples of transition metal (TM) catalysis.[1] While palladium has been the metal of choice for the vast majority of catalytic cross-coupling processes involving the oxidative addition of organohalides,[2] more expensive platinum(0) catalysts have found applications in some specialised cross-coupling reactions, including the coupling of polyfluoroarylimines with $ZnMe_2$,[3] thiolates with (hetero)aryl iodides,[4] hydrazones with allyl halides,[5] or hydrosilanes with iodoalkanes.[6]

Whereas the oxidative addition of carbon–halide bonds and their heavier group 14 congeners at mononuclear Pt(0) complexes has been studied in detail,[7,8] studies of E–X (E = group 14 element, X = halide) bond activations by dinuclear platinum complexes, which may offer unique cooperative reactivity and catalytic enhancement,[9] remain rare. Our group has studied the oxidative addition of (di)boron halides to the diplatinum(0) complex [(μ-dmpm)$_2$Pt$_2$(nbe)$_2$] (**1**, dmpm = bis(dimethylphosphino)methane, nbe = norbornene),[10–12] which offers a flexible platform for the cooperative oxidative addition of B–X bonds at both Pt centres, generating so-called A-frame complexes[13] with a bridging (di)boranediyl apex ligand, like $\mathbf{I^X}$ (Fig. 1A). A number of cooperative activations of organodihalides by similar dppm-bridged (dppm = bis(diphenylphosphino)methane) dinickel(0) and dipalladium(0) systems have been reported, affording a range of organodiyl-bridged A-frame complexes, like the methylene- or vinylidene-

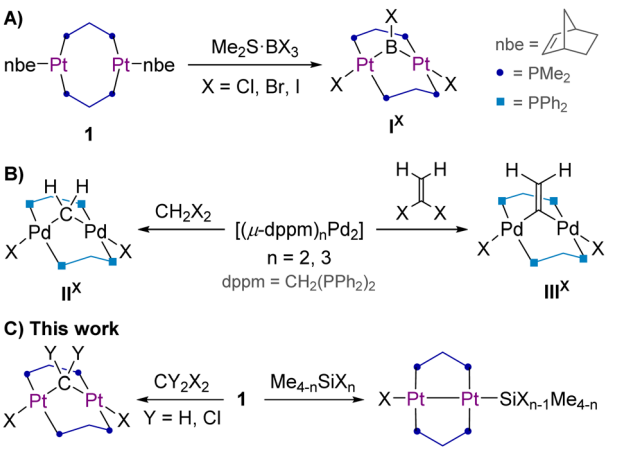

Fig. 1 Cooperative addition of (A) trihaloboranes at the diplatinum(0) complex **1**, (B) organodihalides at a dipalladium(0) complex, and (C) di- and tetrahalomethanes and heavier group 14 halides at **1**.

[a]*Institute for Inorganic Chemistry, Julius-Maximilians-Universität Würzburg, Am Hubland, 97074 Würzburg, Germany*

[b]*Institute for Sustainable Chemistry & Catalysis with Boron, Julius-Maximilians-Universität Würzburg, Am Hubland, 97074 Würzburg, Germany*

[c]*Department of Chemistry and Pharmaceutical Sciences, Amsterdam Institute of Molecular and Life Sciences (AIMMS), Vrije Universiteit Amsterdam, De Boelelaan 1108, 1081 HZ Amsterdam, The Netherlands. E-mail: F.M.Bickelhaupt@vu.nl*

[d]*Institute for Molecules and Materials, Radboud University, Heyendaalseweg 135, 6525 AJ Nijmegen, The Netherlands*

[e]*Department of Chemical Sciences, University of Johannesburg, Auckland Park, Johannesburg 2006, South Africa*

bridged complexes $\mathbf{II}^{\mathbf{X}}$ and $\mathbf{III}^{\mathbf{X}}$.[14] To our knowledge, however, there have been no reports of cooperative activation of organodihalides, let alone heavier group 14 dihalides, by dinuclear group 10 systems.

In this contribution, we present our investigation into the oxidative addition of di- and tetrahalomethanes at **1** and compare it to that of their heavier group 14 counterparts, underpinning the experimental results by DFT calculations on the origin of the differences in reactivity.

Results and discussion

Synthesis of methylene-bridged diplatinum A-frame complexes

Equimolar reactions of **1** with CH_2X_2 (X = Cl, Br) in benzene at room temperature (rt) for 5 min yielded the methylene-bridged platinum(II) A-frame complexes $[(\mu\text{-dmpm})_2Pt_2X_2(\mu\text{-}CH_2)]$ ($\mathbf{2^{CH2}}$-**X**) as yellow solids in high isolated yield (75% each, Scheme 1a). To avoid the use of light-sensitive and potentially mutagenic CH_2I_2, the brown complex $\mathbf{2^{CH2}}$-**I** was synthesised quantitatively by treating $\mathbf{2^{CH2}}$-**Br** with an excess of trimethylsilyl iodide (Scheme 1b). It is noteworthy that all three complexes $\mathbf{2^{CH2}}$-**X** decompose both in solution and when subjected to vacuum to the diplatinum(I) complexes $[(\mu\text{-dmpm})_2Pt_2X_2]$, as has also been observed for boranediyl-bridged diplatinum A-frames under comparable conditions.[10–12] While we are yet to determine the fate of the lost methylene fragment in these decomposition reactions, its spontaneous release from the A-frame complexes $\mathbf{2^{CH2}}$-**X** could potentially be harnessed for metal-mediated C–C bond forming reactions in the presence of suitable substrates, such as azoalkanes, alkenes, alkynes and nucleophilic heterocycles.[15] Coupled with a reductive step to reduce the by-product $[(\mu\text{-dmpm})_2Pt_2X_2]$ back to a diplatinum(0) complex, such processes could even be made catalytic.

While the addition of CCl_4 to **1** also led to the instant formation of the corresponding, orange-coloured dichloromethylene-bridged A-frame complex $\mathbf{2^{CCl2}}$-**Cl** in near-quantitative yield, the latter was only partially characterised as it decomposed rapidly in solution to a range of unidentified complexes.

The ^{1}H NMR spectra of $\mathbf{2^{CH2}}$-**X** show a quintet ($^2J_{H-P} \approx 9$ Hz) with ^{195}Pt satellites ($^1J_{H-Pt} = 55$–58 Hz) for the protons of the bridging methylene, which is shifted upfield with increasing halide electronegativity ($\delta = 0.83$ ($\mathbf{2^{CH2}}$-**Cl**), 1.07 ($\mathbf{2^{CH2}}$-**Br**), 1.47 ($\mathbf{2^{CH2}}$-**I**) ppm), as in the series of analogous dipalladium A-frames $\mathbf{II}^{\mathbf{X}}$.[14] A similar multiplet ($\delta_{1H} = 1.08$ ppm, $^2J_{H-P} \approx 9$ Hz, $^1J_{H-Pt} \approx 54$ Hz) was observed for the analogous $[(\mu\text{-dppm})_2Pt_2Cl_2(\mu\text{-}CH_2)]$, synthesised in 1985 from the reaction of highly explosive diazomethane with the cationic diplatinum complex $[(\mu\text{-dppm})_2\{Pt(PPh_3)\}\{PtH\}]^+$, and subsequent recrystallisation from CH_2Cl_2.[16] The chemical shift of the corresponding high-field $^{13}C\{^1H\}$ NMR multiplet shows a similar trend ($\delta = -14.5$ ($\mathbf{2^{CH2}}$-**Cl**), -7.6 ($\mathbf{2^{CH2}}$-**Br**), 4.5 ($\mathbf{2^{CH2}}$-**I**) ppm), the $^1J_{C-Pt}$ coupling remaining relatively unchanged ($^1J_{C-Pt} = 613$–617 Hz) over the entire series. As expected, the methylene ^{13}C NMR resonance of $\mathbf{2^{CCl2}}$-**Cl** is shifted to much lower field at 20.3 ppm. Conversely, the $^{31}P\{^1H\}$ NMR singlet of $\mathbf{2^{CH2}}$-**X**, with its typical higher-order A-frame satellite splitting pattern ($^1J_{P-Pt} \approx 2980$–3070 Hz, $^3J_{P-Pt} \approx 70$ Hz), is shifted upfield upon descending the halide group (from $\delta = -7.3$ ($\mathbf{2^{CH2}}$-**Cl**) to -13.2 ($\mathbf{2^{CH2}}$-**I**) ppm), as expected with decreasing halide electronegativity (Table 1). The $^{31}P\{^1H\}$ NMR resonance of $\mathbf{2^{CCl2}}$-**Cl** appears at -8.7 ppm, between those of $\mathbf{2^{CH2}}$-**Cl** and $\mathbf{2^{CH2}}$-**Br**, and displays a much lower $^1J_{P-Pt}$ coupling of 2750 Hz but significantly higher $^3J_{P-Pt}$ coupling of 150 Hz. An upfield shift is also observed for the $^{195}Pt\{^1H\}$ NMR triplet of $\mathbf{2^{CH2}}$-**X** upon going down the halide group (from $\delta = -4267$ ppm ($\mathbf{2^{CH2}}$-**Cl**) to -4645 ($\mathbf{2^{CH2}}$-**I**) ppm), concomitant with a decrease in their $^1J_{Pt-P}$ coupling constants (from $^1J_{Pt-P} = 3081$ ($\mathbf{2^{CH2}}$-**Cl**) to 2981 ($\mathbf{2^{CH2}}$-**I**) Hz). The $^{195}Pt\{^1H\}$ NMR triplet of $\mathbf{2^{CCl2}}$-**Cl** was detected by ^1H–^{195}Pt HMQC at -4270 ppm, close to that of $\mathbf{2^{CH2}}$-**Cl**. The analysis of the ^{195}Pt satellite pattern of the $^{31}P\{^1H\}$ NMR multiplets of $\mathbf{2^{CH2}}$-**X** (see Fig. S2 in the SI)[17] enables the determination of the $^2J_{Pt-Pt}$ coupling constants, which decrease from 842 Hz in $\mathbf{2^{CH2}}$-**Cl** to 754 Hz in $\mathbf{2^{CH2}}$-**I**, and are similar to that of $\mathbf{I^{Cl}}$ ($^2J_{Pt-Pt} = 879$ Hz).[11] We have shown that the value of the $^2J_{Pt-Pt}$

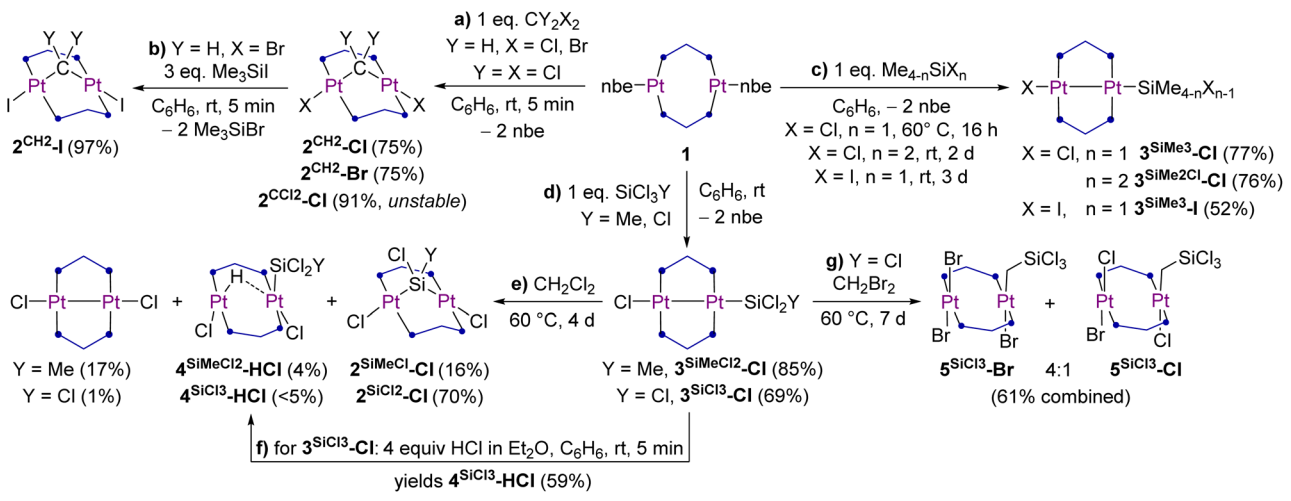

Scheme 1 Reactivity of **1** towards halomethanes and halosilanes.

Table 1 ^{31}P and ^{195}Pt NMR shifts (ppm) and coupling constants (Hz) for the complexes presented herein

	$^{31}P_{P1}$	$^{31}P_{P2}$	$^{1}J_{P1-Pt1}$	$^{1}J_{P2-Pt2}$	$^{n}J_{P1-Pt2}$	$^{n}J_{P2-Pt1}$	$^{195}Pt_{Pt1}$	$^{195}Pt_{Pt2}$	$^{n}J_{Pt-Pt}$
2^{CH2}-Cl	−7.3	—	3072	—	73[a]	—	−4267	—	842[b]
2^{CH2}-Br	−9.6	—	3036	—	71[a]	—	−4397	—	831[b]
2^{CH2}-I	−13.2	—	2982	—	68[a]	—	−4645	—	754[b]
2^{Cl2}-Cl	−8.7	—	2750	—	150	—	−4270	—	n.d.[d]
2^{SiMeCl}-Cl	−0.1[e]	−2.8[f]	3261	3114	261[a]	203[a]	−4519	—	n.d.
2^{SiCl2}-Cl	1.2	—	3098	—	242[a]	—	−4446	—	297[b]
3^{SiMe3}-Cl	−15.6	−25.7	3156	2671	122[b]	48[b]	−4317	−4798	3060[c]
3^{SiMe3}-I	−21.4	−26.5	3132	2656	116[b]	57[b]	−4686	−4755	n.d.
$3^{SiMe2Cl}$-Cl	−17.5	−26.4	3035	2581	138[b]	52[b]	−4309	−4748	3269[c]
$3^{SiMeCl2}$-Cl	−17.7	−26.0	2930	2475	154[b]	57[b]	−4329	−4752	3738[c]
3^{SiCl3}-Cl	−19.4	−26.7	2815	2434	154[b]	62[b]	−4305	−4791	4163[c]
5^{SiCl3}-Br	−20.7	−15.0	2420	2702	n.d.	n.d.	−4408	−4421	—
5^{SiCl3}-Cl	−16.7	−9.6	2420	2720	n.d.	n.d.	−4367	−4411	—

[a] $n = 3$. [b] $n = 2$. [c] $n = 1$. [d] n.d. = not determined due to lack of spectral resolution. [e] P1/P3. [f] P2/P4.

constant in the boranediyl-bridged complexes $[(\mu\text{-dmpm})_2Pt_2X_2(\mu\text{-BY})]$ (X = halide; Y = halide, amino, organo) decreases as the Pt···Pt distance increases, which is also the case in the methylene-bridged A-frame series **2^{CH2}-X** (*vide infra*).

The formation of **2^{CH2}-Cl** and **2^{CH2}-Br** was accompanied by the precipitation of a yellow solid, which in the case of the reaction with CH_2Br_2 was identified by single-crystal X-ray diffraction (SCXRD) analysis as the bis(methylene)-bridged di-platinum(IV) complex $[(\mu\text{-dmpm})_2Pt_2Br_4(\mu\text{-}CH_2)_2]$ (**2^{CH2}-Br′**) (Fig. 2), in which one CH_2Br_2 molecule has added on each side of the $(\mu\text{-dmpm})_2Pt_2$ core. Unfortunately, the reaction of **1** with a large excess of CH_2Br_2 did not yield **2^{CH2}-Br′** more selectively. Although further characterisation of these side-products was marred by their insolubility in all common organic solvents, it is noteworthy that **2^{CH2}-Br′** is a unique example of a dinuclear group 10 complex bridged by two methylene units.

Crystals of **2^{CH2}-Cl**, **2^{CH2}-Br** and **2^{CH2}-I** were also analysed by SCXRD (Fig. 2 and Table 2, see Fig. S67 and S70 in the SI for **2^{CH2}-Cl** and **2^{CH2}-I**). The degree of A-frame distortion in these complexes is quantified by their $|P\text{–}M\text{–}M\text{–}P|_{cis}$ and $|P\text{–}M\text{–}M\text{–}P|_{trans}$ torsion angles (M = metal centre), which amount to 0° and 180°, respectively, in the ideal A-frame structure. Complexes **2^{CH2}-X** all show a relatively small degree of A-frame distortion ($|P\text{–}Pt\text{–}Pt\text{–}P|_{cis} \leq 19°$; $|P\text{–}Pt\text{–}Pt\text{–}P|_{trans} \geq 163°$), while the centrosymmetric structure of **2^{CH2}-Br′** provides a near-ideal A-frame ($|P\text{–}Pt\text{–}Pt\text{–}P|_{cis}$ 1.19(5)°; $|P\text{–}Pt\text{–}Pt\text{–}P|_{trans}$ 180°). The distortion in **2^{CH2}-X** is higher than in their haloboranediyl-bridged counterparts **I^X** ($|P\text{–}Pt\text{–}Pt\text{–}P|_{cis} \leq 7°$; $|P\text{–}Pt\text{–}Pt\text{–}P|_{trans} \geq 173°$), as the more acute Pt–C–Pt angle (**2^{CH2}-X** avg. 100°; **I^X** Pt–B–Pt 111–126°) enforces a shorter Pt···Pt distance (**2^{CH2}-X** avg. 3.15 Å; **I^X** 3.25–3.47 Å).[10] Moreover, the $^{2}J_{Pt-Pt}$ coupling constant decreases (from 842 (**2^{CH2}-Cl**) to 754 (**2^{CH2}-I**) Hz) in line with the increasing Pt···Pt distance (from 3.1475(5) (**2^{CH2}-Cl**) to 3.1745(5) (**2^{CH2}-I**) Å). The Pt–C bond lengths in **2^{CH2}-X** are all similar (avg. 2.06 Å) and consistent with those previously reported for a similar methylene-bridged complex $[(\mu\text{-dppm})_2Pt_2Cl_2(\mu\text{-}CH_2)]$ (2.008(13) Å).[18]

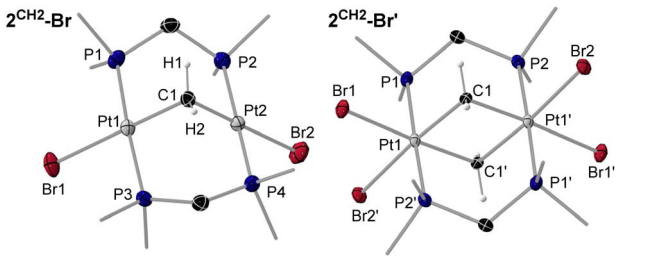

Fig. 2 SCXRD-derived solid-state structures of 2^{CH2}-Br and 2^{CH2}-Br′. Atomic displacement ellipsoids are set at 50%. Ellipsoids of methyl groups and hydrogen atoms are omitted for clarity, except for the protons of the bridging methylene units.

Transannular oxidative addition of methylhalosilanes

There are no literature precedents for the oxidative addition of heavier group 14 halides at dinuclear platinum complexes. The reaction of **1** with $Me_{4-n}SiCl_n$ ($n = 1$–4) provided the transannular oxidative addition products $[(\mu\text{-dmpm})_2\{PtX\}\{Pt(SiMe_{4-n}X_{n-1})\}]$ (X = Cl, $n = 1$: **3^{SiMe3}-Cl** (brown), $n = 2$: **$3^{SiMe2Cl}$-Cl** (beige), $n = 3$: **$3^{SiMeCl2}$-Cl** (yellow), $n = 4$: **3^{SiCl3}-Cl** (yellow); X = I, $n = 1$: **3^{SiMe3}-I** (orange)), in which one Si–X bond has formally added across the central Pt_2 unit (Scheme 1c and d).† Except for the reaction with Me_3SiCl, which required heating at 60 °C for 16 h, all these reactions proceeded at rt. After workup, the resulting silyldiplatinum complexes were isolated in moderate to excellent yields (69–84%). Unlike the A-frame complexes **2^{CY2}-X** the silyldiplatinum complexes **$3^{SiMe(3-n)Xn}$-X** ($n = 0$–3) were stable in solution over longer periods of time. While mononuclear silyl platinum(II) complexes are key intermediates in the catalytic addition of Si–E (E = H, Si, B) bonds to alkenes and alkynes, as well in the silylation of aryl halides,[19] the use of bimetallic complexes or of halosilane precursors in such transformations have not yet been has not been studied.

The $^{29}Si\{^{1}H\}$ NMR spectra of **3^{SiMe3}-Cl** and **3^{SiMe3}-I** display a triplet of triplets ($^{2}J_{Si-P} \approx 10$ Hz, $^{3}J_{Si-P} \approx 2$–4 Hz) with ^{195}Pt satellites, while **$3^{SiMeCl2}$-Cl** and **3^{SiCl3}-Cl** only show coupling to the adjacent phosphines.‡ As expected, the $^{29}Si\{^{1}H\}$ NMR resonances of the chloro derivatives are progressively deshielded (from $\delta = -11$ to 45 ppm) as the number of chlorides increases at the silicon centre. The $^{1}J_{Si-Pt}$ and $^{2}J_{Si-Pt}$ coupling

Table 2 Selected bond lengths (Å), bond angles (°) and torsion angles (°) of the complexes characterised by SCXRD

	P–Pt	Pt–X	Pt···Pt	Pt1–E	Pt2–E	Pt–E–Pt	|P–Pt–Pt–P|$_{cis}$	|P–Pt–Pt–P|$_{trans}$
2^{CH2}-Cl	2.267(2)–2.294(2)	2.4445(19), 2.4351(19)[a]	3.1475(5)	2.060(7)[d]	2.054(7)[d]	99.8(3)[d]	12.01(7), 18.61(7)	163.02(7), 166.36(7)
2^{CH2}-Br	2.2764(17)–2.2864(17)	2.5606(7), 2.5606(7)[b]	3.1604(4)	2.055(6)[d]	2.051(6)[d]	100.7(2)[d]	6.80(6), 13.54(6)	169.69(6), 169.98(6)
2^{CH2}-Br′	2.3419(16), 2.3417(16)	2.6099(12), 2.5811(8)[b]	3.1816(10)	2.079(5)[d]	2.077(5)[d]	99.9(2)[d]	1.19(5)	180
2^{CH2}-I	2.279(3), 2.288(3)	2.7358(7), 2.7129(6)[c]	3.1745(5)	2.057(9)[d]	2.063(8)[d]	100.8(3)[d]	7.7(2), 9.2(1)	170.4(2), 172.6(1)
2^{SiCl2}-Cl	2.2928(16)–2.3054(17)	2.4486(16), 2.4366(16)[a]	3.5682(6)	2.2610(17)[e]	2.2541(17)[e]	104.42(7)[e]	2.28(6), 7.87(6)	161.05(6), 171.20(6)
3^{SiMe3}-I	2.2542(19)–2.2714(19)	2.7402(6)[c]	2.7320(5)	—	2.357(2)[e]	—	52.27(7), 54.80(7)	125.15(7), 127.78(7)
3^{SiMe2Cl}-Cl	2.2501(19)–2.2796(17)	2.4419(18)[a]	2.6921(7)	—	2.3316(18)[e]	—	53.68(6), 55.83(6)	125.23(6), 125.26(6)
3^{SiMeCl2}-Cl	2.2562(19)–2.2798(18)	2.4402(17)[a]	2.6897(6)	—	2.2960(18)[e]	—	52.67(6), 54.89(6)	126.19(7), 126.24(6)
3^{SiCl3}-Cl	2.2576(9)–2.2897(8)	2.4195(9)[a]	2.66556(18)	—	2.2933(9)[e]	—	53.14(3), 55.79(3)	125.39(3), 125.67(3)
4^{SiCl3}-HCl	2.278(3)–2.330(3)	2.420(3), 2.397(3)[a]	3.1734(9)	—	2.253(3)[e]	—	14.2(1), 28.4(1)	157.5(1), 159.9(1)
5^{SiCl3}-Br	2.2959(16)–2.3073(17)	2.4403(7)–2.4968(7)[b]	3.400(1)	2.097(6)[d]	—	—	12.21(7), 12.61(7)	163.88(7), 171.30(7)

[a] X = Cl. [b] X = Br. [c] X = I. [d] E = C. [e] E = Si.

constants increase with the number of halides at silicon, from 990 and 273 Hz, respectively, in **3^{SiMe2Cl}-Cl** to 1629 and 624 Hz, respectively, in **3^{SiCl3}-Cl**. The same trends have been observed for the ^{29}Si{^{1}H} NMR chemical shifts and $^{1}J_{Si–Pt}$ constants in the mononuclear disilylplatinum complexes [(Et$_3$P)$_2$Pt(SiMe$_{3-n}$Cl$_n$)$_2$] (n = 0–2). The ^{31}P{^{1}H} NMR spectra of **3$^{SiMe(3–n)Xn}$-X** reflect the asymmetry of the complexes, showing two higher-order multiplets with complex satellite patterns around −26 ppm for the P$_2$*Pt*Si nuclei and −15 to −19 ppm for the P$_2$*Pt*Cl nuclei, or −21 ppm for the P$_2$*Pt*I nucleus. The influence of the *trans*-silyl ligand in the chloro derivatives induces a small but non-negligible upfield shift in the P$_2$*Pt*Cl resonance as the degree of chlorination of the silyl ligand increases, as also observed in [(Et$_3$P)$_2$Pt(SiMe$_{3-n}$Cl$_n$)Cl] (n = 0–2).[20] While the *Pt*Si centres in **3$^{SiMe(3–n)Xn}$-X** all display a similar ^{195}Pt{^{1}H} NMR shift, between −4740 and −4800 ppm, the resonance of the *Pt*I centre in **3^{SiMe3}-I** (δ = −4686 ppm) is significantly upfield-shifted compared to that of the *Pt*Cl centre in the chloro derivatives ($\delta \approx$ −4300 to −4330 ppm), as already observed in **2^{CH2}-X**. In the chloro derivatives the $^{1}J_{Pt–Pt}$ coupling constants increase from 3060 Hz to 4163 Hz, both with the degree of chlorination of the silyl ligand and a shortening of the Pt–Pt bond length (*vide infra*). These $^{1}J_{Pt–Pt}$ coupling constants are relatively small compared to other unsymmetrical bis(diphosphine)-bridged diplatinum(I) complexes displaying Pt–Pt bonding, such as the stannyl analogue of **3^{SiCl3}-Cl**, [(μ-dppm)$_2${PtCl}{Pt(SnCl$_3$)}] (obtained from the reaction of [(μ-dppm)$_2$Pt$_2$Cl$_2$] with SnCl$_2$, $^{1}J_{Pt–Pt}$ = 8200 Hz),[21] [(μ-dppm)$_2$Pt$_2$Cl$_2$] ($^{1}J_{Pt–Pt}$ = 8146 Hz),[22] or our [(μ-dmpm^{tab})(μ-dmpm)Pt$_2$Br$_2$] complexes (dmpm^{tab} = tetrazaborolyl-substituted dmpm ligand, $^{1}J_{Pt–Pt}$ = 6670–8510 Hz).[23]

Colourless crystals of **3^{SiMe2Cl}-Cl**, and yellow crystals of **3^{SiMe3}-I**, **3^{SiMeCl2}-Cl** and **3^{SiCl3}-Cl**, provided suitable data for SCXRD analysis (Fig. 3 and 4, left, and Table 2; see Fig. S71 and S72 in the SI for **3^{SiMe3}-I** and **3^{SiMe2Cl}-Cl**). As exemplified in the right-hand view of complex **3^{SiMeCl2}-Cl** in Fig. 3, the (μ-dmpm)$_2$Pt$_2$ frameworks of these complexes are highly distorted (|P–Pt–Pt–P|$_{cis}$ 52–56°, |P–Pt–Pt–P|$_{trans}$ 125–128°). Indeed, a CCDC search shows these are the most distorted [(μ-CH$_2${-PR$_2$}$_2$)$_2$Pt$_2$XY] complexes that have been reported, beside the twisted isomers of our recent [(μ-dmpm^{tab})(μ-dmpm)Pt$_2$Br$_2$] complexes (|P–Pt–Pt–P|$_{cis}$ 49–52°, |P–Pt–Pt–P|$_{trans}$ 126–132°),[23] and [(μ-dmpm)$_2$Pt$_2$Br$_2$] (|P–Pt–Pt–P|$_{cis}$ 49°, |P–Pt–Pt–P|$_{trans}$ 124–

Fig. 3 Two views of the SCXRD-derived solid-state structures of **3^{SiMeCl2}-Cl**, highlighting its twisted framework. Atomic displacement ellipsoids are set at 50%. Ellipsoids of phosphine-bound methyl groups and hydrogen atoms are omitted for clarity.

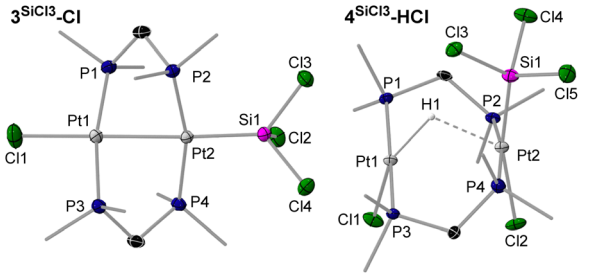

Fig. 4 SCXRD-derived solid-state structures of 3^{SiCl3}-Cl and 4^{SiCl3}-HCl. Atomic displacement ellipsoids are set at 50%. Ellipsoids of methyl groups and hydrogen atoms are omitted for clarity, except for the bridging hydride in 4^{SiCl3}-HCl.

136°).[10] The Pt–Pt bond lengths range from 2.66556(18) Å in **3^{SiCl3}-Cl** to 2.7320(5) Å in **3^{SiMe3}-I**, in the typical range for neutral [{μ-$CH_2(PR_2)_2$}$_2$$Pt_2$XY] complexes (2.62–2.71 Å).[10,24] They also decrease with the degree of chlorination of the silyl ligand, as more electron density is pulled out of the Pt–Pt bond. Similarly, the Pt–Si distance also decreases with the degree of silyl chlorination, from 2.2933(9) in **3^{SiCl3}-Cl** to 2.357(2) Å in **3^{SiMe3}-I**. Similar Pt–Si bond lengths are found in mononuclear, unchelated [*trans*-$(R_3P)_2$PtX(SiR′$_3$)] complexes (2.32–2.39 Å).[25]

Transannular oxidative additions like these, with concomitant metal–metal bond formation, were first reported by Schmidbaur in 1975 at a cyclometallated dinuclear Au(II) complex using elemental halogens and methyl iodide.[26] Other examples of transannular oxidative additions of group 14 halides have been reported for dinuclear Au(I), Au(II), Ir(I) and Rh(I) complexes,[27–29] but remain limited to alkyl halides. Similarly, Brown and Puddephatt reported the oxidative addition of alkyl iodides at [(μ-dppm)$_3$$Pt_2$], which yielded the ionic Pt(I)$_2$ complexes [(μ-dppm)$_2${(η^1-dppm)Pt}{PtR}]I, in which a terminally coordinated dppm ligand takes the place of the iodide.[30]

Solvent-dependent reactivity of $3^{SiMeCl2}$-Cl and 3^{SiCl3}-Cl

During the full NMR-spectroscopic characterisation of both **$3^{SiMeCl2}$-Cl** and **3^{SiCl3}-Cl** in CD_2Cl_2, the appearance of two new products was observed after several hours at rt (Scheme 1e). The minor one was identified by SCXRD as **$4^{SiMeCl2}$-HCl** and **4^{SiCl3}-HCl**, respectively, the product of the transannular addition of HCl, possibly derived from traces of HCl present from the degradation of the dichloromethane solvent through either hydrolysis, photolysis or Pt-catalysed oxidation with trace oxygen.[31] The major one was identified as the rearrangement product **2^{SiMeCl}-Cl** and **2^{SiCl2}-Cl**, respectively, *i.e.* the corresponding silylene-bridged A-frame complex. Complexes **$4^{SiMeCl2}$-HCl** and **4^{SiCl3}-HCl** were systematically detected in small amounts (<5%) in dichloromethane solutions of **$3^{SiMeCl2}$-Cl** and **3^{SiCl3}-Cl**, respectively. For full characterisation **4^{SiCl3}-HCl** was synthesised independently by the addition of 1 equiv. HCl in Et_2O to **3^{SiCl3}-Cl** (Scheme 1f). In the $^{31}P\{^1H\}$ NMR spectra, **$4^{SiMeCl2}$-HCl** and **4^{SiCl3}-HCl** appear as two multiplets around −7 to −9 ppm (P_2PtHCl) and −14 ppm (P_2PtSiCl), and in the $^{195}Pt\{^1H\}$ NMR spectra as two multiplets around −4600 and −4700 ppm, as also confirmed by ^1H–^{195}Pt $\{^1H\}$ HSQC experiments. The ^1H NMR spectrum of **4^{SiCl3}-HCl** shows a highly shielded Pt*H* triplet at −15.8 ppm ($^2J_{H-P}$ = 13.2 Hz), with satellites to the two Pt nuclei ($^1J_{H-Pt}$ = 1193 Hz, $^3J_{H-Pt}$ = 22.8 Hz). These values are similar to those of the mononuclear [*trans*-$(Me_3P)_2$PtHCl], which shows a Pt*H* triplet at −16.2 ppm ($^2J_{H-P}$ = 17 Hz), with a slightly larger coupling to the adjacent Pt nucleus ($^1J_{H-Pt}$ = 1308 Hz).[32]

The solid-state structure of **4^{SiCl3}-HCl** confirms the transannular oxidative addition of HCl at **3^{SiCl3}-Cl** (Fig. 4, right). The Pt···Pt distance of 3.1734(9) Å is similar to that of the A-frame complexes **2^{CH2}-X**, thus precluding any Pt–Pt bonding. As a result, the (μ-dmpm)$_2$$Pt_2$ framework is much less distorted than in **3^{SiCl3}-Cl** ($|P–Pt–Pt–P|_{cis} \leq 28.4(1)°$, $|P–Pt–Pt–P|_{trans} \geq 157.5(1)°$). The bridging hydride, located in the inverse Fourier map and freely refined, bridges very unsymmetrically between the Pt centres (Pt1–H1 1.87(11), Pt2···H1 2.23(11) Å). To our knowledge, **4^{SiCl3}-HCl** is the first example of a neutral hydrido-diplatinum(II) complex, the only reported cationic one being the symmetrical complex [(μ-dmpm)$_2$$Pt_2$$Me_2$(μ-H)]$^+$, with a significantly shorter Pt···Pt distance 2.932(1) Å, the hydride not having been located in that structure.[33]

Whereas **3^{SiCl3}-Cl** fully rearranged to the μ-silylene A-frame complex **2^{SiCl2}-Cl** over 4 days at 60 °C in CH_2Cl_2, enabling its isolation in 70% yield, the rearrangement of **$3^{SiMeCl2}$-Cl** to **2^{SiMeCl}-Cl** remained incomplete, reaching only 17%, and was accompanied by the formation of the decomposition product [(μ-dmpm)$_2$$Pt_2Cl_2$] (Scheme 1e). Like its methylene-bridged analogues, **2^{SiCl2}-Cl** proved unstable in solution, decomposing spontaneously to [(μ-dmpm)$_2$$Pt_2Cl_2$] with release of the:$SiCl_2$ unit, the exact fate of which was not ascertained. As such, **2^{SiCl2}-Cl** may provide an interesting starting point for studying platinum-mediated or -catalysed silylene transfer reactions, which are usually performed using silirane precursors.[34]

Complex **2^{SiCl2}-Cl** shows a ^{29}Si NMR triplet with Pt satellites at 22.5 ppm ($^2J_{Si-P}$ = 10.2 Hz, $^1J_{Si-Pt}$ = 1559 Hz), *ca.* 20 ppm upfield-shifted compared to the terminal silyl resonance of **$3^{SiMeCl2}$-Cl** (δ = 44.6 ppm). The $^{31}P\{^1H\}$ NMR singlet of **2^{SiCl2}-Cl** at 1.2 ppm is *ca.* 10 ppm upfield-shifted from that of its dichloromethylene-

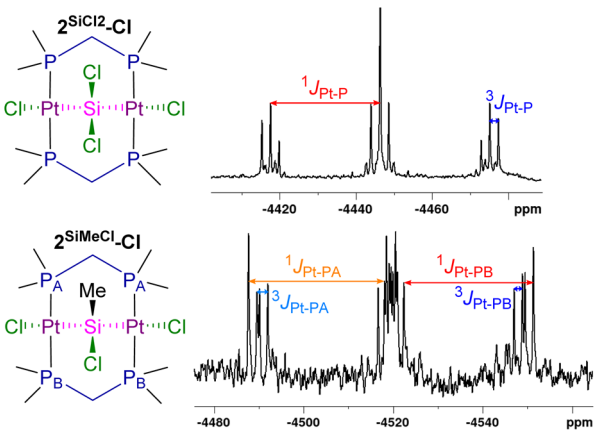

Fig. 5 $^{195}Pt\{^1H\}$ spectra of 2^{SiCl2}-Cl and 2^{SiMeCl}-Cl.

bridged analogue **2^{CCl2}-Cl** ($\delta = -8.7$ ppm), as the silylene is more electron-donating than the methylene ligand. Both the $^{1}J_{P-Pt}$ (3098 (**2^{SiCl2}-Cl**), 2750 (**2^{CCl2}-Cl**) Hz) and $^{3}J_{P-Pt}$ (242 (**2^{SiCl2}-Cl**), 150 (**2^{CCl2}-Cl**) Hz) coupling constants increase significantly upon changing from the CCl_2 to the $SiCl_2$ bridge. Interestingly, complex **2^{SiMeCl}-Cl** displays two 1 : 1 $^{31}P\{^{1}H\}$ NMR triplets at −0.1 and −2.8 ppm, rather than a singlet. This is owed to the asymmetry generated by the SiMeCl bridge, as the methyl and chloride substituents each point to one of the dmpm ligands, thereby creating slightly different magnetic environments. The ^{195}Pt NMR triplet of **2^{SiCl2}-Cl** at −4446 ppm is also upfield-shifted from **2^{CCl2}-Cl** ($\delta = -4270$ ppm), while its $^{3}J_{Pt-Pt}$ coupling constant is substantially lower than that of all the methylene-bridged A-frames ($^{3}J_{Pt-Pt} = 297$ (**2^{SiCl2}-Cl**), 750–842 (**2^{SiCH2}-X**) Hz),§ in line with the larger Pt⋯Pt distance in **2^{SiCl2}-Cl** (*vide infra*). For **2^{SiMeCl}-Cl** the asymmetry generated by the SiMeCl bridge results in a dddd resonance at −4519 ppm in the $^{195}Pt\{^{1}H\}$ NMR spectrum, with two distinct $^{1}J_{Pt-P}$ (3261, 3114 Hz) and $^{3}J_{Pt-P}$ (261, 203 Hz) coupling constants to each of the dmpm ligands (Fig. 5).

Green crystals of **2^{SiCl2}-Cl** were analysed by SCXRD (Fig. 6, left). The much larger covalent radius of the silicon compared to the carbon bridge ($r_{Si} = 1.11$ Å, $r_{C} = 0.76$ Å) induces a significant widening of the Pt⋯Pt distance (3.5682(6) Å) compared to **2^{CH2}-Cl** (3.1475(5) Å), which in turn releases the strain of the (μ-dmpm)$_2$Pt$_2$ framework, resulting in a nearly ideal A-frame structure ($|P–Pt–Pt–P|_{cis} \leq 7.87(6)$, $|P–Pt–Pt–P|_{trans} \geq 161.05(6)°$). The Pt–Si bonds in **2^{SiCl2}-Cl** (2.2610(17), 2.2541(17) Å) are significantly shorter than in the silyl complexes **3$^{SiMe(3-n)Xn}$-X** (2.2933(9)–2.357(2) Å), or other silylene-bridged diplatinum complexes with square-planar Pt coordination environments (2.2998(11)–2.412(2) Å).[35,36] This shortening is likely due to the strain imposed by the A-frame and the electron-withdrawing effect of the chlorides *trans* to the silylene.

While there are numerous examples of silylene-bridged di- and triplatinum(0) complexes, usually synthesised by dehydrogenation of dihydrosilanes or the direct addition of stable silylenes to the Pt(0) precursors,[37] our silylene-bridged A-frames are the first examples of μ-silylene diplatinum(II) complexes, obtained by twofold Si–X oxidative addition at two Pt(0) centres. There are, however, a couple of examples of homo- and heterobimetallic μ-silylene platinum(II) complexes obtained by the oxidative addition of the Si–H bond of a hydrosilyl ligand to a Pt centre.[36] In these cases, the bridging SiR_2 ligand should rather be viewed as a triplet silanediyl ligand with electron-sharing Pt–Si bonds, rather than a singlet silylene with Si→Pt donor–acceptor bonding. The same observation has been made for our BY-bridged A-frame complexes, which should be regarded as boranediyl-rather than borylene-bridged complexes.

While in CH_2Cl_2 complex **3^{SiCl3}-Cl** rearranges to **2^{SiCl2}-Cl**, in CH_2Br_2 the unsymmetrical silyl(trihalo)diplatinum(II) complexes **5^{SiCl3}-Br** and **5^{SiCl3}-Cl** are formed, in which a unique twofold oxidative addition of CH_2Br_2, concomitant with methylene insertion into the Pt–Si bond, and in the case of **5^{SiCl3}-Br** an additional Cl–Br exchange, have taken place. The two products were formed in a 4 : 1 mixture, as determined by NMR spectroscopy, and could not be separated by fractional crystallisation (Scheme 1g). Both species were detected by HRMS, and **5^{SiCl3}-Br** was additionally characterised by SCXRD (*vide infra*). In the ^{1}H NMR spectrum complexes **5^{SiCl3}-Br** and **5^{SiCl3}-Cl** show a distinctive P_2PtCH_2 2H triplet at 1.74 and 2.35 ppm ($^{2}J_{H-P} = 8.5$ Hz), respectively, corresponding to a shielded $^{13}C\{^{1}H\}$ NMR Pt*C*H$_2$ multiplet at −1.2 ppm. In the $^{29}Si\{^{1}H\}$ NMR spectrum both compounds overlap at 2.5 ppm. The $^{31}P\{^{1}H\}$ NMR spectrum shows two triplets for each complex, reflecting their asymmetry, one set at −15.0 ($P_2PtBr(CH_2SiCl_3)$) and −20.7 (P_2PtBr_2) ppm for **5^{SiCl3}-Br** ($^{2}J_{P-P} = 11.8$ Hz), and one at −9.6 ($P_2PtCl(CH_2SiCl_3)$) and −16.7 ($P_2PtBrCl$) ppm for **5^{SiCl3}-Cl** ($^{2}J_{P-P} = 15.2$ Hz), with $^{1}J_{P-Pt}$ coupling constants of *ca.* 2400 Hz for the P_2PtX_2 moiety and *ca.* 2700 Hz for the $P_2PtX(CH_2SiCl_3)$ moiety. These assignments are based on comparison with the ^{31}P NMR data of the mononuclear complexes *trans*-[(Me$_3$P)$_2$PtX$_2$] (X = Cl, $\delta = -15.8$ ppm, $^{1}J_{P-Pt} = 2386$ Hz; X = Br, $\delta = -21.5$ ppm, $^{1}J_{P-Pt} = 2324$ Hz),[38] and *trans*-[(Me$_3$P)$_2$Pt(CH$_2$SiMe$_3$)Cl] ($\delta = -14.6$ ppm, $^{1}J_{P-Pt} = 2765$ Hz).[39] The orientation of the Cl and Br ligands at the first Pt centre in **5^{SiCl3}-Cl** relative to the CH_2SiCl_3 ligand of the second Pt centre remains unclear, as no single crystals of **5^{SiCl3}-Cl** could be obtained.

The solid-state structure of **5^{SiCl3}-Br** (Fig. 6, right) shows two near-parallel square-planar Pt centres (Pt1 ∠ Pt2 *ca.* 3°) bridged by two dmpm ligands, one bearing two bromides and the other a bromide and a CH_2SiCl_3 ligand. The Pt⋯Pt distance of 3.400(1) Å is significantly shorter than in the related complex *trans*-[(μ-dmpm)$_2$Pt$_2$I$_4$] (Pt⋯Pt 3.3477(6) Å).[11] The Pt2–C1 bond length of 2.091(6) Å is similar to that of the related *trans*-[(Me$_2$PhP)$_2$PtCl(CH$_2$SiMe$_3$)] (2.079(14) Å).[40]

Insertion reactions of unsaturated hydrocarbons into Pt–Si bonds represent a key step in the Pt-catalysed hydrosilylation of alkenes and alkynes.[41] To our knowledge, however, there have been no reports of methylene insertions into a Pt–Si bond. Puddephatt and coworkers have studied a similar insertion of methylene into the Pt–aryl bond of a cycloneophylplatinum(II) complex upon addition of CH_2X_2 (X = Cl, Br, I), which was calculated to proceed *via* a radical mechanism.[42] Others have reported ionic reaction mechanisms of chloromethyl platinum(II) complexes involving the displacement of the chloride anion by various Lewis bases (LB) and formation of new Pt–CH_2–LB linkages (E = PR_3, SR_2, NR_n).[43]

Based on these studies, it is possible that the formation of **5^{SiCl3}-Cl** proceeds first *via* a formal transannular, likely radical oxidative addition of Br$^{\bullet}$ and $^{\bullet}CH_2Br$, yielding the unstable

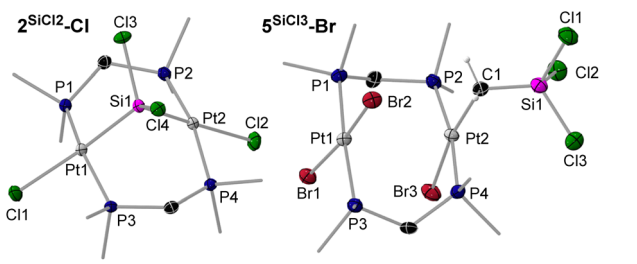

Fig. 6 SCXRD-derived solid-state structures of **2^{SiCl2}-Cl** and **5^{SiCl3}-Br**. Atomic displacement ellipsoids are set at 50%. Ellipsoids of methyl groups and hydrogen atoms are omitted for clarity, except for the methylene protons in **5^{SiCl3}-Br**.

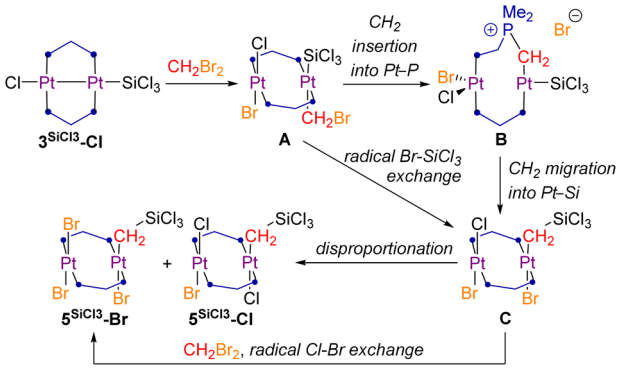

Scheme 2 Possible mechanisms for the formation of 5^{SiCl3}-X from 3^{SiCl3}-Cl and CH_2Br_2.

trans-(bromomethyl)silyl complex **A** (Scheme 2). Subsequent insertion of the CH_2 unit into one of the Pt–P bonds and displacement of the bromide anion yields the phosphonium ylide **B** (or its dicationic Pt–Pt-bonded analogue if the second bromide also gets displaced). Complex **B** then undergoes CH_2 migration into the Pt–Si bond, with concomitant reformation of the Pt–P bond and bromide addition to Pt2, yielding the silyl(-trihalo)diplatinum(II) complex **C**. Alternatively, a radical Br–$SiCl_3$ exchange at **A** could lead directly to **C**. Finally, **C** undergoes radical or ionic disproportionation to $\mathbf{5^{SiCl3}}$**-Cl** and $\mathbf{5^{SiCl3}}$**-Br**, or radical Cl–Br exchange to yield the observed excess of $\mathbf{5^{SiCl3}}$**-Br.**

Comparative computational study of the reactivity of 1 with CH_2Cl_2, CCl_4 and $SiCl_4$

In order to understand the divergent reactivity of **1** towards dihalomethanes and polychlorosilanes, quantum-chemical calculations using density functional theory (DFT) were undertaken. All computations were performed at the ZORA[44]-BLYP[45]-D3(BJ)[46]/TZ2P[47] level of theory, using the conductor-like screening model (COSMO)[48] to simulate solvation in benzene (see the full computational details in the SI). This level of theory has been proven to be accurate for studying bond activation by group 10 metals and metal–metal interactions, both in previous reports,[49,50] as well as in the additional performance test carried out in the current work (see details in the SI). The optimised structures of $\mathbf{2^{CH2}}$**-Cl** and $\mathbf{3^{SiCl3}}$**-Cl** at this level of theory are in good agreement with the experimental SCXRD-derived structures, notwithstanding small discrepancies attributable to the fact that the computed structures are optimised in solution rather than the solid state (see Fig. S78 in the SI).

In order to identify the origin of the divergent reactivity of **1** towards CY_2Cl_2 (Y = H, Cl) and $SiCl_4$, the relative stability of the two possible isomeric products, *i.e.* the methylene/silylene-bridged A-frame, and the product of transannular C/Si–Cl addition, was first investigated. The optimised geometries and relative energies are presented in Fig. 7. In all three cases the A-frame complex is the most stable species and thus corresponds to the thermodynamic product. This aligns with the experimentally observed eventual rearrangement of $\mathbf{3^{SiCl3}}$**-Cl** to $\mathbf{2^{SiCl2}}$**-Cl** upon prolonged heating in CH_2Cl_2. It is noteworthy that the

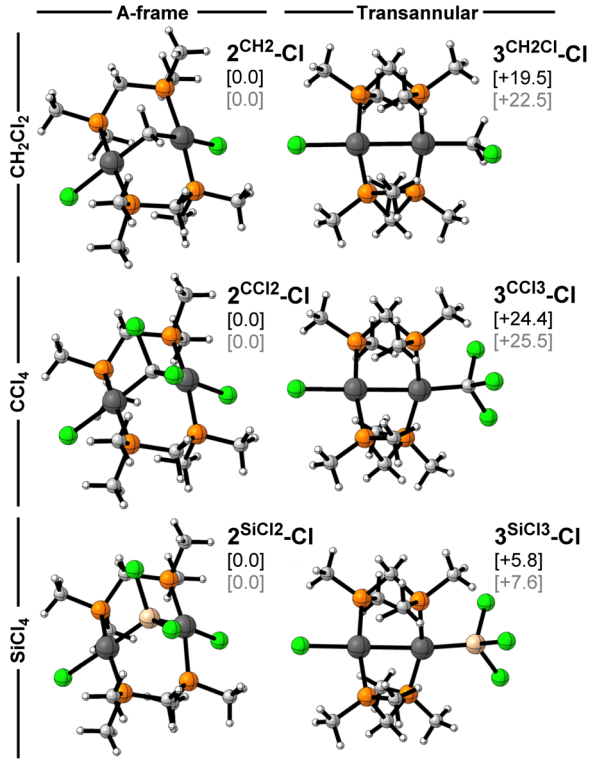

Fig. 7 Ball-and-stick structures, relative Gibbs free energies ΔG (in black, kcal mol^{-1}), and relative electronic energies ΔE (in grey, kcal mol^{-1}) of the optimised A-frame (left) and transannular oxidative addition (right) products of CH_2Cl_2, CCl_4, and $SiCl_4$ with complex **1**, calculated at the COSMO(benzene)-ZORA-BLYP-D3(BJ)/TZ2P level of theory. Atom colours: H = white; C = grey; P = orange; Cl = green; Si = beige; Pt = anthracite.

energetic preference for the A-frame is significantly more pronounced for the halomethanes ($\Delta G \geq 19.5$ kcal mol^{-1}) than the halosilane ($\Delta G = 5.8$ kcal mol^{-1}), which is consistent with the sole observation of the A-frame product in the former systems.

Although the A-frame product is thermodynamically favoured, all halosilane substrates yield the transannular diplatinum(I) complex at rt, which is therefore the kinetic product, associated with the lowest activation barrier in the selectivity-determining step. This is confirmed by our DFT calculations, which reveal two distinct two-step reaction mechanisms, one for the transannular oxidative addition of $SiCl_4$ to **1**, yielding $\mathbf{3^{SiCl3}}$**-Cl** (TA pathway in blue, Fig. 8a), and the other for the direct twofold oxidative addition, yielding the A-frame $\mathbf{2^{SiCl2}}$**-Cl** (AF pathway in red, Fig. 8a). In both cases $SiCl_4$ first coordinates to **1** with release of the nbe ligands to form a hypervalent reactant complex (RC), a typical feature of silicon chemistry that cannot be accessed by the halocarbon analogues.[51] This can occur either on one side of the diplatinum complex, yielding the transannular RC (**TA-RC**), or in the centre above the Pt···Pt unit, yielding the A-frame RC (**AF-RC**, Fig. 8b). The nature of the [$SiCl_4$···**1**] interaction in both reactant complexes was assessed in more detail using quantitative energy decomposition analysis (see Table S1 in the SI).[52] The

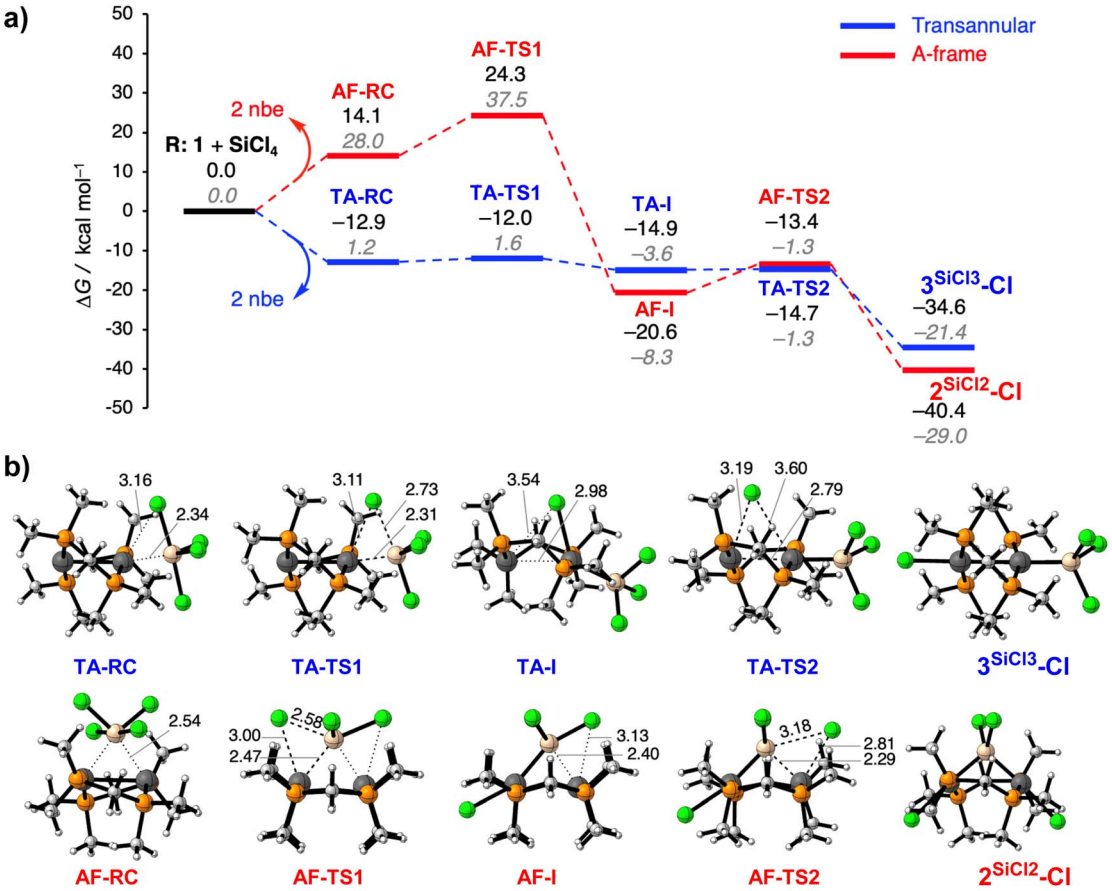

Fig. 8 (a) Reaction profiles of the transannular addition (TA, blue pathway) and direct A-frame formation (AF, red pathway) of $SiCl_4$ with **1**. Relative Gibbs free energies ΔG (in kcal mol^{-1}) and electronic energies ΔE (in grey italics). (b) Corresponding stationary point structures with relevant bond lengths (in Å). All computations were carried out at the COSMO(benzene)-ZORA-BLYP-D3(BJ)/TZ2P level of theory. R = reactants; RC = reactant complex; TS = transition state; I = intermediate. Note that the fourth chlorine atom of $SiCl_4$ appears hidden in the orientation of **AF-TS1**, **AF-I**, and **AF-TS2**.

results show that the electrostatic and orbital interactions are the main stabilising bonding components in both complexes and of similar magnitude. The main difference lies in the higher steric Pauli repulsion experienced by **AF-RC** as the $SiCl_4$ molecule sits atop the centre of **1**, rather than on one side. As a result, the formation of **TA-RC** is exergonic by $\Delta G_1 = -12.9$ kcal mol^{-1}, whereas that of **AF-RC** is endergonic by $\Delta G_1 = +14.1$ kcal mol^{-1}. Note that CCl_4 and CH_2Cl_2 cannot form reactant complexes of this nature because the central carbon atom cannot become hypervalent, and the C–Cl bonds are relatively shorter and too rigid to allow this degree of bond angle deformation. Instead, CCl_4 and CH_2Cl_2 form a reactant complex by coordinating on top of **1** through one of the Cl atoms (see Fig. S79 in the SI), thereby favouring an AF pathway.

Once the RC is formed, both pathways proceed with the selectivity-determining step, the oxidative addition of one Si–Cl bond at one of the Pt centres (Fig. 8a). In the corresponding transition-state (TS) structure of the AF pathway, **AF-TS1**, the $SiCl_4$ moiety is highly deformed, resulting in a very high overall first activation barrier of $\Delta G_1^{\ddagger} = +24.3$ kcal mol^{-1}. In contrast, the TS structure of the first oxidative addition of the TA pathway, **TA-TS1**, strongly resembles that of **TA-RC**, resulting in a very low first activation barrier of $\Delta G_1^{\ddagger} = +0.9$ kcal mol^{-1}. In both cases an intermediate mixed-valence Pt(II)–Pt(0) complex is formed, in which the Pt(0) centre remains dicoordinate and the Pt(II) centre displays a distorted square-planar geometry, with either the silyl (**AF-I**) or the chloride (**TA-I**) ligand positioned above the Pt···Pt unit. While the formation of **AF-I** from **AF-RC** is highly exergonic ($\Delta G_2 = -34.7$ kcal mol^{-1}), that of **TA-I** from **TA-RC** is only mildly so ($\Delta G_2 = -2.0$ kcal mol^{-1}), making the latter process actually reversible. While the AF pathway is thus highly thermodynamically favoured, the TA pathway is kinetically much more accessible, and therefore always preferred.

In the AF pathway **AF-I** then undergoes a second Si–Cl bond addition at the remaining Pt(0) centre *via* **AF-TS2** yielding the silylene-bridged $\mathbf{2^{SiCl2}}$**-Cl**, with a much lower barrier than for the first addition ($\Delta G_2^{\ddagger} = +7.2$ kcal mol^{-1}). In the TA pathway the transfer of the second chloride to the second Pt centre, which yields $\mathbf{3^{SiCl3}}$**-Cl**, is virtually barrierless ($\Delta G_2^{\ddagger} = +0.2$ kcal mol^{-1}). Consequently, the TA pathway is kinetically favoured for both reaction steps. Formation of the thermodynamically favoured silylene-bridged A-frame $\mathbf{2^{SiCl2}}$**-Cl** could only be achieved by heating $\mathbf{3^{SiCl3}}$**-Cl** in CH_2Cl_2 for four days (see Scheme 1e). The kinetic preference for the TA product is expected to be even more

pronounced for the methylsilyl derivatives, as the larger methyl groups would render the formation of **AF-RC** and **AF-TS1** even less favourable. In addition, the non-coordinating and larger methyl groups likely decrease, or even invert, the thermodynamic preference for the AF relative to the TA pathway, as additional steric clashes between the silane and Pt complex methyl groups would induce even larger Pauli repulsion in the AF reactant complexes and transition states (see SI Table S1). As a result, only $\mathbf{3^{SiCl3}}$**-Cl** fully rearranges to $\mathbf{2^{SiCl2}}$**-Cl**, whereas $\mathbf{3^{SiMeCl2}}$**-Cl** rearranges only partially, and $\mathbf{3^{SiMe2Cl}}$**-Cl** and $\mathbf{3^{SiMe3}}$**-Cl** do not.

Conclusion

We demonstrated in this work the unique cooperative reactivity that a dinuclear platinum complex, $[(\mu\text{-dmpm})_2Pt_2(nbe)_2]$ (**1**), exhibits towards the double activation of C–X and Si–X bonds of CH_2X_2 (X = Cl, Br, I), CCl_4 and $Me_{4-n}SiX_n$ (X = Cl, n = 1–4; X = I, n = 1), respectively. Upon reaction with di- and tetrahalomethanes, complex **1** exclusively forms methylene-bridged A-frame structures ($\mathbf{2^{CY2}}$**-X**), while halosilanes undergo transannular oxidative addition reactions in which one Si–X bond is added across the two metal centres, leading to the formation of unsymmetrical silyldiplatinum(I) complexes ($\mathbf{3^{SiMe(3-n)Xn}}$**-X**). Upon heating in dichloromethane the transannular addition product of **1** and $SiCl_4$, complex $\mathbf{3^{SiCl3}}$**-Cl**, fully rearranges to the corresponding silylene-bridged A-frame complex $\mathbf{2^{SiCl2}}$**-Cl**, while its $MeSiCl_3$-derived analogue, $\mathbf{3^{SiMeCl2}}$**-Cl**, undergoes only partial rearrangement. In contrast, heating in dibromomethane results in a highly unusual insertion of a CH_2Br_2-derived methylene unit into the Pt–Si bond ($\mathbf{5^{SiCl3}}$**-X**).

DFT computations reveal that the methylene/silylene-bridged A-frame complexes are always the thermodynamic products, albeit with a much stronger preference for the A-frames in the halomethane-based reactions. For $SiCl_4$ the direct two-step formation of the A-frame complex $\mathbf{2^{SiCl2}}$**-Cl** has a much higher activation barrier than the pathway leading to the kinetic transannular addition product $\mathbf{3^{SiCl3}}$**-Cl**. The propensity towards rearrangement of the transannular addition product $\mathbf{3^{SiMe(3-n)Cln}}$**-Cl** to the A-frame is dictated by the number of methyl groups, as these clash with the dmpm methyl groups during the rearrangement.

The divergent reaction pathways described herein highlight the potential of bimetallic complexes in tuning cooperative bond activations, which could be integrated into new methylene/silylene transfer or silylation reactions. Further investigations to broaden the substrate scope and ultimately harness the cooperativity of these diplatinum complexes in catalytic transformations are underway in our laboratory.

Author contributions

M. P. designed the study, carried out the experimental work and wrote the SI. C. N. carried out and wrote the computational contributions. M. A. wrote the manuscript. H. B. and M. B. provided supervision and funding.

Conflicts of interest

The authors declare no conflict of interest.

Data availability

CCDC 2406490 ($\mathbf{2^{CH2}}$**-Cl**), 2406494 ($\mathbf{2^{CH2}}$**-Br**), 2406498 ($\mathbf{2^{CH2}}$**-I**), 2406509 ($\mathbf{2^{CH2}}$**-Br′**), 2406550 ($\mathbf{3^{SiMe3}}$**-I**), 2406556 ($\mathbf{3^{SiMe2Cl}}$**-Cl**), 2406558 ($\mathbf{3^{SiMeCl2}}$**-Cl**), 2406564 ($\mathbf{3^{SiCl3}}$**-Cl**), 2505905 ($\mathbf{4^{SiCl3}}$**-HCl**), 2406843 ($\mathbf{2^{SiCl2}}$**-Cl**) and 2406901 ($\mathbf{5^{SiCl3}}$**-Br**) contain the supplementary crystallographic data for this paper.[54a–k]

The data supporting this article have been included as part of the supplementary information (SI). Supplementary information: methods, synthetic procedures, NMR spectra, X-ray crystallographic and computational details. See DOI: https://doi.org/10.1039/d6sc00337k.

Acknowledgements

The authors thank Mr Christoph Maler for mass-spectroscopic and Dr Rüdiger Bertermann for NMR-spectroscopic analyses. Financial support from the Julius-Maximilians-Universität Würzburg, as well as funding from the Deutsche Forschungsgemeinschaft (DFG project number 466754611) is gratefully acknowledged. C. N. and F. M. B. thank the Dutch Research Council (NWO) for financial support and SURF Cooperative and VU ADA for the computational resources.

Notes and references

† In order to study silicon–halide bond activation, methylhalosilanes were chosen instead of dihydrodihalosilanes (SiH_2X_2) as the Si–H bond is significantly weaker than the Si–X bond,[53] resulting in preferential Si–H activation in test reactions with $SiHCl_3$ and Me_2SiHCl.

‡ The $^{29}Si\{^1H\}$ NMR signal for $\mathbf{3^{SiCl3}}$**-Cl** was too weak to be detected.

§ The $^2J_{Pt-Pt}$ coupling constant of $\mathbf{2^{CCl2}}$**-Cl** could not be determined due to poor spectral resolution.

1 Selected reviews: (*a*) N. Chatani, *Chem.-Asian J.*, 2025, **20**, e00808; (*b*) K. M. Korch and D. A. Watson, *Chem. Rev.*, 2019, **119**, 8192–8228; (*c*) D. J. Jones, M. Lautens and G. P. McGlacken, *Nat. Catal.*, 2019, **2**, 843–851; (*d*) D. J. Weix, *Acc. Chem. Res.*, 2015, **48**, 1767–1775; (*e*) N. Kambe, T. Iwasakia and J. Terao, *Chem. Soc. Rev.*, 2011, **40**, 4937–4947; (*f*) J. K. Stille and K. S. Y. Lau, *Acc. Chem. Res.*, 1977, **10**, 434–442.

2 Selected reviews: (*a*) I. P. Beletskaya and A. V. Cheprakov, *Chem. Rev.*, 2000, **100**, 3009–3066; (*b*) C. Cordovilla, C. Bartolome, J. M. Martínez-Ilarduya and P. Espinet, *ACS Catal.*, 2015, **5**, 3040–3053; (*c*) F. Bellina, A. Carpita and R. Rossi, *Synthesis*, 2004, **15**, 2419–2440; (*d*) R. Chinchilla and C. Nájera, *Chem. Rev.*, 2007, **107**, 874–922.

3 T. Wang, B. J. Alfonso and J. A. Love, *Org. Lett.*, 2007, **9**, 5629–5631.

4 H. Kuniyasu, F. Yamashita, T. Hirai, J.-H. Ye, S.-I. Fujiwara and N. Kambe, *Organometallics*, 2006, **25**, 566–570.

5 J.-T. Hong and H.-Y. Jang, *J. Org. Chem.*, 2011, **76**, 6877–6882.

6 H. Inubushi, H. Kondo, A. Lesbani, M. Miyachi, Y. Yamanoi and H. Nishihara, *Chem. Commun.*, 2013, **49**, 134–136.
7 (*a*) S. Kozuch, C. Amatore, A. Jutand and S. Shaik, *Organometallics*, 2005, **24**, 2319–2330; (*b*) T. Nishida, S. Ogoshi, K. Tsutsumi, Y. Fukunishi and H. Kurosawa, *Organometallics*, 2000, **19**, 4488–4491; (*c*) A. L. Casado and P. Espinet, *Organometallics*, 1998, **17**, 954–959; (*d*) H. Kurosawa, H. Kajimaru, S. Ogoshi, H. Yoneda, K. Miki, K. Kasai, S. Murai and I. Ikeda, *J. Am. Chem. Soc.*, 1992, **114**, 8417–8424; (*e*) M. F. Lappert and P. W. Lednor, *J. Chem. Soc. Chem. Commun.*, 1973, 948–949.
8 (*a*) H. Yamashita, T. Hayashi, T. Kobayashi, M. Tanaka and M. Goto, *J. Am. Chem. Soc.*, 1988, **110**, 4417–4418; (*b*) C. J. Levy, R. J. Puddephatt and J. J. Vittal, *Organometallics*, 1994, **13**, 1559–1560; (*c*) H. Yamashita, T.-A. Kobayashi, M. Tanaka, J. A. Samuels and W. E. Streib, *Organometallics*, 1992, **11**, 2330–2333; (*d*) T. A. K. Al-Allaf, *J. Organomet. Chem.*, 1999, **590**, 25–35; (*e*) C. Eaborn, A. Pidcock and B. R. Steele, *J. Chem. Soc., Dalton Trans.*, 1976, 767–776; (*f*) J. Kuyper, *Inorg. Chem.*, 1977, **16**, 2171–2176; (*g*) S. M. Nabavizadeh, F. Niroomand Hosseini, N. Nejabat and Z. Parsa, *Inorg. Chem.*, 2013, **52**, 13480–13489.
9 (*a*) M. Navarro, J. J. Moreno, M. Pérez-Jiménez and J. Campos, *Chem. Commun.*, 2022, **58**, 11220–11235; (*b*) R. Maity, B. S. Birenheide, F. Breher and B. Sarkar, *Chem. – Eur. J.*, 2021, **13**, 2337–2370; (*c*) B. M. Trost, C.-I. Hung and G. Matac, *Angew. Chem., Int. Ed.*, 2020, **59**, 4240–4261; (*d*) J. Parka and S. Hong, *Chem. Soc. Rev.*, 2012, **41**, 6931–6943.
10 C. Brunecker, J. H. Müssig, M. Arrowsmith, F. Fantuzzi, A. Stoy, J. Böhnke, A. Hofmann, R. Bertermann, B. Engels and H. Braunschweig, *Chem. – Eur. J.*, 2020, **26**, 8518–8523.
11 C. Brunecker, M. Arrowsmith, J. H. Müssig, J. Böhnke, A. Stoy, M. Heß, A. Hofmann, C. Lenczyk, C. Lichtenberg, J. Ramler, A. Rempel and H. Braunschweig, *Dalton Trans.*, 2021, **50**, 3506–3515.
12 C. Brunecker, M. Arrowsmith, F. Fantuzzi and H. Braunschweig, *Angew. Chem., Int. Ed.*, 2021, **60**, 16864–16868.
13 (*a*) D. M. Hoffmann and R. Hoffmann, *Inorg. Chem.*, 1981, **20**, 3543–3555; (*b*) C. P. Kubiak and R. Eisenberg, *J. Am. Chem. Soc.*, 1977, **99**, 6129–6131.
14 (*a*) E. Lumbreras Jr., E. M. Sisler and Q. D. Shelby, *J. Organomet. Chem.*, 2010, **695**, 201–205; (*b*) S. Hinze, J. K. Gong, P. E. Fanwick and C. P. Kubiak, *J. Organomet. Chem.*, 1993, **458**, C10–C11; (*c*) X. L. R. Fontaine, S. J. Higgins and B. L. Shaw, *J. Chem. Soc., Dalton Trans.*, 1988, 1179–1184; (*d*) S. J. Young, B. Kellenberger, J. H. Reibenspies, S. E. Himmel, M. Manning, O. P. Anderson and J. K. Stille, *J. Am. Chem. Soc.*, 1988, **110**, 5744–5753; (*e*) X. L. R. Fontaine, S. J. Higgins, B. L. Shaw, M. Thornton-Pett and W. Yichang, *J. Chem. Soc., Dalton Trans.*, 1987, 1501–1507; (*f*) A. L. Balch, C. T. Hunt, C.-L. Lee, M. M. Olmstead and J. P. Farr, *J. Am. Chem. Soc.*, 1981, **103**, 3764–3772.
15 (*a*) M. Cowie, *Can. J. Chem.*, 2005, **83**, 1043–1055; (*b*) S. J. Trepanier, J. N. L. Dennett, B. T. Sterenberg, R. McDonald and M. Cowie, *J. Am. Chem. Soc.*, 2004, **126**, 8046–8058; (*c*) M. Akita, R. Hua, S. A. R. Knox, Y. Morooka, S. Nakanishi and M. I. Yates, *J. Organomet. Chem.*, 1998, **569**, 71–83; (*d*) T. B. Gunnoe, P. S. White, J. L. Templeton and L. Casarrubios, *J. Am. Chem. Soc.*, 1997, **119**, 3171–3172; (*e*) P. M. Maitlis, *J. Organomet. Chem.*, 1995, **500**, 239–249.
16 M. P. Brown, J. R. Fisher, R. J. Puddephatt and K. R. Seddon, *Inorg. Chem.*, 1979, **18**, 2808–2813.
17 (*a*) M. C. Grossel, J. R. Batson, R. P. Moulding and K. R. Seddon, *J. Organomet. Chem.*, 1986, **304**, 391–423; (*b*) M. P. Brown, R. J. Puddephatt, L. Rashidi and K. R. Seddon, *J. Chem. Soc., Dalton Trans.*, 1978, 516–522.
18 K. A. Azam, A. A. Frew, B. R. Lloyd, L. Manojlovic-Muir, K. W. Muir and R. J. Puddephatt, *Organometallics*, 1985, **4**, 1400–1406.
19 (*a*) R. Yu. Lukin, A. M. Kuchkaev, A. V. Sukhov, G. E. Bekmukhamedov and D. G. Yakhvarov, *Polymers*, 2020, **12**, 2174; (*b*) D. Troegel and J. Stohrer, *Coord. Chem. Rev.*, 2011, **255**, 1440–1459; (*c*) A. Hamze, O. Provot, M. Alami and J.-D. Brion, *Org. Lett.*, 2006, **8**, 931–934; (*d*) F. Ozawa, *J. Organomet. Chem.*, 2000, **611**, 332–342; (*e*) M. Tanaka, Y. Uchimaru and H.-J. Lautenschlager, *Organometallics*, 1991, **10**, 16–18; (*f*) T. Hayashi, T.-a. Kobayashi, A. M. Kawamoto, H. Yamashlta and M. Tanaka, *Organometallics*, 1990, **9**, 280–281.
20 A. Roscher, A. Bockholt and T. Braun, *Dalton Trans.*, 2009, 1378–1382.
21 M. C. Grossel, R. P. Moulding and K. R. Seddon, *Inorg. Chim. Acta Lett.*, 1982, **64**, L275–L277.
22 K. A. Brittingham and S. Schreiner, *J. Chem. Educ.*, 1995, **72**, 941–943.
23 M. Passargus, M. Arrowsmith, R. Bertermann, M. Finze and H. Braunschweig, *Inorg. Chem.*, 2025, **64**, 21111–21129.
24 N. I. Khan, C. King, J.-C. Wang, S. Wang and J. P. Fackler Jr., *Inorg. Chem.*, 1989, **28**, 4656–4662.
25 (*a*) P. Kapoor, K. Lövqvist and Å. Oskarsson, *Acta Crystallogr., Sect. C: Cryst. Struct. Commun.*, 1995, **51**, 611–613; (*b*) Y.-J. Kim, J.-I. Park, S.-C. Lee, K. Osakada, M. Tanabe, J.-C. Choi, T.-A. Koizumi and T. Yamamoto, *Organometallics*, 1999, **18**, 1349–1352.
26 H. Schmidbaur and R. Franke, *Inorg. Chim. Acta*, 1975, **13**, 85–89.
27 (*a*) H. E. Abdou, A. A. Mohamed and J. P. Fackler Jr., *Inorg. Chem.*, 2007, **46**, 9692–9699; (*b*) J. D. Basil, H. Murray, J. P. Fackler Jr., J. Tocher, A. M. Mazany, B. Trzcinska-Bancroft, H. Knachel, D. Dudis, T. J. Delord and D. O. Marler, *J. Am. Chem. Soc.*, 1985, **107**, 6908–6915; (*c*) H. Schmidbaur and P. Jandik, *Inorg. Chim. Acta*, 1983, **74**, 97–99.
28 (*a*) M. T. Pinillos, A. Elduque, J. A. Lopez, F. J. Lahoz and L. A. Oro, *J. Chem. Soc., Dalton Trans.*, 1991, 1391–1395; (*b*) M. A. Ciriano, J. J. Pérez-Torrente and L. A. Oro, *J. Organomet. Chem.*, 1993, **445**, 273–281.
29 (*a*) M. P. Brown, A. Yavari, R. H. Hill and R. J. Puddephatt, *J. Chem. Soc., Dalton Trans.*, 1985, 2421–2425; (*b*) K. A. Azam, M. P. Brown, R. H. Hill, R. J. Puddephatt and A. Yavari, *Organometallics*, 1984, **3**, 697–702.

30 N. S. Lewis, K. R. Mann, J. G. Gordon II and B. Gray, *J. Am. Chem. Soc.*, 1976, **98**, 7461–7463.
31 (*a*) I. Fells and E. A. Moelwyn-Hughes, *J. Chem. Soc.*, 1958, 1326–1333; (*b*) M. E. Jacox and D. E. Milligan, *J. Chem. Phys.*, 1970, **53**, 2688–2701; (*c*) L. Pinard, J. Mijoin, P. Ayrault, C. Canaff and P. Magnoux, *Appl. Catal. B Environ.*, 2004, **51**, 1–8.
32 D. L. Packett, C. M. Jensen, R. L. Cowan, C. E. Strouse and W. C. Trogler, *Inorg. Chem.*, 1985, **24**, 3578–3583.
33 M. P. Brown, S. J. Cooper, A. A. Frew, L. Manojlović-Muir, K. W. Muir, R. J. Puddephatt and M. A. Thomson, *J. Chem. Soc., Dalton Trans.*, 1982, 299–305.
34 (*a*) Z. Nevárez and K. A. Woerpel, *Org. Lett.*, 2007, **9**, 3773–3776; (*b*) M. A. Greene, M. Prévost, J. Tolopilo and K. A. Woerpel, *J. Am. Chem. Soc.*, 2012, **134**, 12482–12484; (*c*) Z. Li and C. He, *Eur. J. Org Chem.*, 2006, 4313–4322.
35 (*a*) M. Tanabe, Y. Nakamura, T.-a. Niwa, M. Sakai, A. Kaneko, H. Toi, K. Okuma, Y. Tsuchido, T.-a. Koizumi, K. Osakada and T. Ide, *Organometallics*, 2022, **41**, 3301–3312; (*b*) M. Tanabe, J. Jiang, H. Yamazawa, K. Osakada, T. Ohmura and M. Suginome, *Organometallics*, 2011, **30**, 3981–3991; (*c*) H. Arii, M. Takahashi, M. Nanjo and K. Mochida, *Dalton Trans.*, 2010, **39**, 6434–6440; (*d*) J. Braddock-Wilking, J. Y. Corey, K. A. Trankler, K. M. Dill, L. M. French and N. P. Rath, *Organometallics*, 2004, **23**, 4576–4584; (*e*) K. A. Brittingham, T. N. Gallaher and S. Schreiner, *Organometallics*, 1995, **14**, 1070–1072.
36 J. Braddock-Wilking, Y. Levchinsky and N. P. Rath, *Inorg. Chim. Acta*, 2002, **330**, 82–88.
37 (*a*) S. Shimada, M. L. N. Rao, Y. Hua Li and M. Tanaka, *Organometallics*, 2005, **24**, 6029–6036; (*b*) J. Powell, J. F. Sawyer and M. Shiralian, *Organometallics*, 1989, **8**, 577–583.
38 R. Favez, R. Roulet, A. A. Pinkerton and D. Schwarzenbach, *Inorg. Chem.*, 1980, **19**, 1356–1365.
39 R. Kapadia, J. B. Pedley and G. B. Young, *Inorg. Chim. Acta*, 1997, **265**, 235–239.
40 B. Jovanović, L. Manojlović-Muir and K. W. Muir, *J. Chem. Soc., Dalton Trans.*, 1974, 195–198.
41 (*a*) K. M. Lewis and S. Couderc, *Molecules*, 2022, **27**, 4341; (*b*) P. Gigler, M. Drees, K. Riener, B. Bechlars, W. A. Herrmann and F. E. Kuhn, *J. Catal.*, 2012, **295**, 1–14; (*c*) I. E. Markó, S. Stérin, O. Buisine, G. Mignani, P. Branlard, B. Tinant and J. P. Declercq, *Science*, 2002, **298**, 204–206; (*d*) A. K. Roy and R. B. Taylor, *J. Am. Chem. Soc.*, 2002, **124**, 9510–9524; (*e*) F. Ozawa, *J. Organomet. Chem.*, 2000, **611**, 332–342.
42 (*a*) M. E. Moustafa, P. D. Boyle and R. J. Puddephatt, *J. Organomet. Chem.*, 2021, **941**, 121803; (*b*) M. A. Fard, A. Behnia and R. J. Puddephatt, *J. Organomet. Chem.*, 2019, **890**, 32–42.
43 (*a*) R. McCrindle, G. J. Arsenault, A. Gupta, M. J. Hampden-Smith, R. E. Rice and A. J. McAlees, *J. Chem. Soc., Dalton Trans.*, 1991, 949–954; (*b*) R. McCrindle, G. Ferguson and A. J. McAlees, *J. Chem. Soc., Chem. Commun.*, 1990, 1524–1526; (*c*) R. McCrindle, G. Ferguson, G. J. Arsenault, M. J. Hampden-Smith, A. J. McAlees and B. L. Rub, *J. Organomet. Chem.*, 1990, **390**, 121–126; (*d*) N. W. Alcock, P. G. Pringle, P. Bergamini, S. Sostero and O. Traverso, *J. Chem. Soc., Dalton Trans.*, 1990, 1553–1556; (*e*) J. F. Hoover and J. M. Stryker, *Organometallics*, 1988, **7**, 2082–2084; (*f*) R. McCrindle, G. J. Arsenault and R. Farwaha, *J. Organomet. Chem.*, 1985, **296**, C51–C53.
44 (*a*) E. van Lenthe, A. Ehlers and E. J. Baerends, *J. Chem. Phys.*, 1999, **110**, 8943–8953; (*b*) E. van Lenthe, E. J. Baerends and J. G. Snijders, *J. Chem. Phys.*, 1994, **101**, 9783–9792.
45 (*a*) A. D. Becke, *Phys. Rev. A*, 1988, **38**, 3098–3100; (*b*) C. Lee, W. Yang and R. G. Parr, *Phys. Rev. B*, 1988, **37**, 785–789; (*c*) Q. Wu and W. Yang, *J. Chem. Phys.*, 2002, **116**, 515–524.
46 (*a*) S. Grimme, *J. Comput. Chem.*, 2004, **25**, 1463–1473; (*b*) S. Grimme, *J. Comput. Chem.*, 2006, **27**, 1787–1799; (*c*) S. Grimme, J. Antony, S. Ehrlich and H. Krieg, *J. Chem. Phys.*, 2010, **132**, 154104; (*d*) S. Grimme, S. Ehrlich and L. Goerigk, *J. Comput. Chem.*, 2011, **32**, 1456; (*e*) A. D. Becke and E. R. Johnson, *J. Chem. Phys.*, 2005, **122**, 154101; (*f*) E. R. Johnson and A. D. Becke, *J. Chem. Phys.*, 2006, **124**, 024101.
47 E. van Lenthe and J. Baerends, *J. Comput. Chem.*, 2003, **24**, 1142–1156.
48 (*a*) A. Klamt and G. Schüürmann, *J. Chem. Soc., Perkin Trans. 2*, 1993, 799–805; (*b*) A. Klamt, *J. Phys. Chem.*, 1995, **99**, 2224–2235; (*c*) C. C. Pye and T. Ziegler, *Theor. Chem. Acc.*, 1999, **101**, 396–408.
49 (*a*) A. Diefenbach and F. M. Bickelhaupt, *J. Phys. Chem. A*, 2004, **108**, 8460–8466; (*b*) G. T. de Jong, M. Solà, L. Visscher and F. M. Bickelhaupt, *J. Chem. Phys.*, 2004, **121**, 9982–9991; (*c*) T. Hansen, X. Sun, M. Dalla Tiezza, W.-J. van Zeist, J. N. P. van Stralen, D. P. Geerke, L. P. Wolters, J. Poater, T. A. Hamlin and F. M. Bickelhaupt, *Chem. – Eur. J.*, 2022, **28**, e202201093; (*d*) J. N. P. van Stralen and F. M. Bickelhaupt, *Organometallics*, 2006, **25**, 4260–4264; (*e*) N. Arnold, R. Bertermann, F. M. Bickelhaupt, H. Braunschweig, M. Drisch, M. Finze, F. Hupp, J. Poater and J. A. P. Sprenger, *Chem. – Eur. J.*, 2017, **23**, 5948–5955.
50 M. B. Brands, J. Nitsch and C. Fonseca Guerra, *Inorg. Chem.*, 2018, **57**, 2603–2613.
51 S. C. A. H. Pierrefixe, C. Fonseca Guerra and F. M. Bickelhaupt, *Chem. – Eur. J.*, 2008, **14**, 819–828.
52 (*a*) F. M. Bickelhaupt and E. J. Baerends, in *Reviews in Computational Chemistry*, ed. K. B. Lipkowitz and D. B. Boyd, Wiley-VCH, New York, 2000, 15, pp. 1–86; (*b*) T. A. Hamlin, P. Vermeeren, C. Fonseca Guerra and F. M. Bickelhaupt, in *Complementary Bonding Analysis*, ed. S. Grabowsky, De Gruyter, Berlin, 2021, 8, pp. 199–212.
53 R. Walsh, *Acc. Chem. Res.*, 1981, **14**, 246–252.
54 (*a*) CCDC 2406490: Experimental Crystal Structure Determination, 2026, DOI: 10.5517/ccdc.csd.cc2ls4q8; (*b*) CCDC 2406494: Experimental Crystal Structure Determination, 2026, DOI: 10.5517/ccdc.csd.cc2ls4vd; (*c*) CCDC 2406498: Experimental Crystal Structure Determination, 2026, DOI: 10.5517/ccdc.csd.cc2ls4zj; (*d*) CCDC 2406509: Experimental Crystal Structure Determination, 2026, DOI: 10.5517/ccdc.csd.cc2ls5bx; (*e*)

CCDC 2406550: Experimental Crystal Structure Determination, 2026, DOI: 10.5517/ccdc.csd.cc2ls6n8; (*f*) CCDC 2406556: Experimental Crystal Structure Determination, 2026, DOI: 10.5517/ccdc.csd.cc2ls6vg; (*g*) CCDC 2406558: Experimental Crystal Structure Determination, 2026, DOI: 10.5517/ccdc.csd.cc2ls6xj; (*h*) CCDC 2406564: Experimental Crystal Structure Determination, 2026, DOI: 10.5517/ccdc.csd.cc2ls73r; (*i*) CCDC 2406843: Experimental Crystal Structure Determination, 2026, DOI: 10.5517/ccdc.csd.cc2lsj31; (*j*) CCDC 2406901: Experimental Crystal Structure Determination, 2026, DOI: 10.5517/ccdc.csd.cc2lskzy; (*k*) CCDC 2505905: Experimental Crystal Structure Determination, 2026, DOI: 10.5517/ccdc.csd.cc2q3ln3.